CHALMERS | UNIVERSITY OF GOTHENBURG

PREPRINT 2010:23

A nonconforming rotated Q_1 approximation on tetrahedra

PETER HANSBO

Department of Mathematical Sciences
Division of Mathematics
CHALMERS UNIVERSITY OF TECHNOLOGY
UNIVERSITY OF GOTHENBURG
Gothenburg Sweden 2010

Preprint 2010:23

A nonconforming rotated Q_1 approximation on tetrahedra

Peter Hansbo

Department of Mathematical Sciences
Division of Mathematics
Chalmers University of Technology and University of Gothenburg
SE-412 96 Gothenburg, Sweden
Gothenburg, April 2010

Preprint 2010:23
ISSN 1652-9715

Matematiska vetenskaper
Göteborg 2010

A nonconforming rotated Q_1 approximation on tetrahedra

Peter Hansbo

Department of Mathematical Sciences, Chalmers University of Technology and University of Gothenburg, S–412 96 Göteborg, Sweden.

Abstract

In this paper we construct an approximation that uses midpoints of edges on tetrahedra in three dimensions. The construction is based on the three–dimensional version of the rotated Q_1–approximation proposed by Rannacher and Turek [5]. We prove *a priori* error estimates for finite element solutions of the elasticity equations using the new element. Since it contains (rotated) bilinear terms it performs substantially better than the standard constant strain element in bending. It also allows for under–integration in near incompressible situations. Numerical examples are included.

1 Introduction

Automatic mesh generation is now standard in commercial software for tetrahedral meshes, whereas completely automated hexahedral meshing remains unsolved. In using low order elements for elasticity applications, the trilinear hexahedral (hex) element has some substantial advantages over the constant strain tetrahedral (tet) element. It performs better in bending (is less prone to "shear locking") on comparable meshes and it allows for under–integration in near incompressibility which allows for avoiding volumetric locking. With automatically generated tet meshes, typically a piecewise quadratic approximation is therefore used. In this paper we show that it is possible to have a type of trilinear approximation also on tet meshes if one accepts that the method is nonconforming. We build our approximation on the rotated Q_1 approximation of Rannacher and Turek [5], a nonconforming method for use on quadrilateral and hex meshes. We prove optimal *a priori* error estimates for the elasticity problem and give numerical evidence of the superior behaviour in bending as well as the effect of under–integration in near incompressibility.

An outline of the paper is as follows: in Section 2 we recall the rotated Q_1 element, based on a reference configuration (unlike [5]), and discuss some

crucial aspects of the approximation on tet elements. In Section 3 we give application to the problem of linearized elasticity, for which we prove optimal convergence. Finally, in Section 4 we give some numerical examples to show the properties of the approximation.

2 The rotated Q_1 approximation

2.1 The 2D case

Consider a subdivision of a bounded region $\Omega \subset \mathbb{R}^2$ into a geometrically conforming finite element partitioning $\mathcal{T}_h = \{K\}$ of Ω consisting of convex quadrilaterals. In Rannacher and Turek [5], there is given the following non-parametric definition of a nonconforming element: for any element $K \in \mathcal{T}_h$, let $(\bar{\xi}, \bar{\eta})$ denote a coordinate system obtained by joining the midpoints of the opposing faces of K, see Fig. 1. On each K we set

$$Q_1^{\mathrm{R}}(K) := \mathrm{span}\{1, \bar{\xi}, \bar{\eta}, \bar{\xi}^2 - \bar{\eta}^2\}.$$

One can now choose what type of continuity one wants. In the following, we shall deal exclusively with enforced continuity at the midpoints of the faces, which is the simplest choice.

There is a parametric version of $Q_1^{\mathrm{R}}(K)$, which means that there exists a reference configuration $\hat{K}$ for the approximation (a fact not noted in [5]). There is also the possibility of expressing the approximation in global coordinates (x, y). To define the reference configuration, we must separate the geometry (based on the usual bilinear map) from the approximation itself. Consider thus a reference element defined for $0 \le \xi \le 1$, $0 \le \eta \le 1$. Using the double numbering of Figure 1, we use numerical subscripts to denote quantities associated with sides, so that $\{\boldsymbol{m}_i\}$ denotes the physical location of the side midpoints, and $\{\phi_i\}$ denotes the nonconforming basis functions, and alphabetical subscripts to denote quantities related to the corners. We now define a local basis for the approximation using the (r, s) system of Fig. 1, with $0 \le r \le 1$, $0 \le s \le 1$, given directly as

$$\phi_1 = (1 - r)(1 - s), \quad \phi_2 = r\,(1 - s), \quad \phi_3 = r\,s, \quad \phi_4 = (1 - r)\,s.$$

It may be more natural to define the basis functions in the (ξ, η) system, however, which can (for instance) be found by rotation and stretch of the

(r, s) system, in inverted form as

$$\begin{bmatrix} r \\ s \end{bmatrix} = \begin{bmatrix} -1/2 \\ 1/2 \end{bmatrix} + \begin{bmatrix} 1 & 1 \\ -1 & 1 \end{bmatrix} \begin{bmatrix} \xi \\ \eta \end{bmatrix},$$

yielding

$$\phi_1 = 3/4 + \xi - \xi^2 - 2\eta + \eta^2,\ \phi_2 = -1/4 + \xi^2 + \eta - \eta^2,$$
$$\phi_3 = -1/4 + \xi - \xi^2 + \eta^2, \qquad \phi_4 = 3/4 - 2\xi + \xi^2 + \eta - \eta^2.$$

In order to compute derivatives of the basis functions, we define a map $\boldsymbol{F} : (\xi, \eta) \to (x, y)$ by

$$(x, y) = \boldsymbol{F}(\xi, \eta) := \sum_i \phi_i(\xi, \eta)\boldsymbol{m}_i.$$

Now, we have that $\boldsymbol{m}_1 = (\boldsymbol{x}_a + \boldsymbol{x}_b)/2$, $\boldsymbol{m}_2 = (\boldsymbol{x}_b + \boldsymbol{x}_c)/2$, $\boldsymbol{m}_3 = (\boldsymbol{x}_c + \boldsymbol{x}_d)/2$ and $\boldsymbol{m}_3 = (\boldsymbol{x}_d + \boldsymbol{x}_a)/2$, so a straightforward computation shows that

$$\boldsymbol{x}(\boldsymbol{\xi}) = \frac{(\boldsymbol{x}_b + \boldsymbol{x}_c - \boldsymbol{x}_a - \boldsymbol{x}_d)\xi}{2} + \frac{(\boldsymbol{x}_c + \boldsymbol{x}_d - \boldsymbol{x}_a - \boldsymbol{x}_b)\eta}{2} + \frac{3\boldsymbol{x}_a + \boldsymbol{x}_b - \boldsymbol{x}_c + \boldsymbol{x}_d}{4}.$$

i.e., *the map $\boldsymbol{F}$ is affine*. The affinity of $\boldsymbol{F}$ implies that we obtain a parallelogram by joining the midpoints of the sides of a general quadrilateral. This is a well known fact first proven by Varignon, cf. Oliver [4]. The proof applies to skew quadrilaterals in spaces of any dimension, a fact that we shall exploit in the following.

2.2 Mapping to the edges of a tetrahedron in 3D

In the three–dimensional case we define the rotated approximation by

$$Q_1^{\mathrm{R}}(\hat{K}) := \mathrm{span}\{1, \xi, \eta, \zeta, \xi^2 - \eta^2, \xi^2 - \zeta^2\},$$

where $\hat{K}$ is the reference configuration $0 \le \xi, \eta, \zeta \le 1$. This gives six unknowns for the six faces of a hexahedron element. We remark that $\eta^2 - \zeta^2 \in Q_1(\hat{K})$ (it can be written as the linear combination $\xi^2 - \zeta^2 - (\xi^2 - \eta^2)$), so all rotated

bilinear terms are still present in the approximation. A nodal basis for $Q_1(\hat{K})$ based on the side numbering in Fig. 2 is readily found as

$$\phi_1 = \frac{1}{3}(2 + 2\,\xi - 7\,\eta + 2\,\zeta - 2\,\xi^2 + 4\,\eta^2 - 2\,\zeta^2),$$
$$\phi_2 = \frac{1}{3}(-1 - \xi + 2\,\eta + 2\,\zeta + 4\,\xi^2 - 2\,\eta^2 - 2\,\zeta^2),$$
$$\phi_3 = \frac{1}{3}(-1 + 2\,\xi - \eta + 2\,\zeta - 2\,\xi^2 + 4\,\eta^2 - 2\,\zeta^2),$$
$$\phi_4 = \frac{1}{3}(2 - 7\,\xi + 2\,\eta + 2\,\zeta + 4\,\xi^2 - 2\,\eta^2 - 2\,\zeta^2),$$
$$\phi_5 = \frac{1}{3}(2 + 2\,\xi + 2\,\eta - 7\,\zeta - 2\,\xi^2 - 2\,\eta^2 + 4\,\zeta^2),$$
$$\phi_6 = \frac{1}{3}(-1 + 2\,\xi + 2\,\eta - \zeta - 2\,\xi^2 - 2\,\eta^2 + 4\,\zeta^2).$$

There are also six edges on a tetrahedron, so we may define a map $\boldsymbol{F} : (\xi, \eta, \zeta) \rightarrow (x, y, z)$ from the reference configuration to the physical tetrahedron by

$$\boldsymbol{x} = \boldsymbol{F}(\boldsymbol{\xi}) := \sum_i \phi_i(\boldsymbol{\xi})\boldsymbol{m}_i,$$

where now $\boldsymbol{m}^i$ denotes the midpoints of the edges on the tetrahedron. Using the numbering of Fig. 3, we find

$$\boldsymbol{x}(\boldsymbol{\xi}) = \boldsymbol{x}_a + \frac{\xi}{2}(-\boldsymbol{x}_a + \boldsymbol{x}_b + \boldsymbol{x}_c - \boldsymbol{x}_d) + \frac{\eta}{2}(-\boldsymbol{x}_a - \boldsymbol{x}_b + \boldsymbol{x}_c + \boldsymbol{x}_d)$$
$$+\frac{\zeta}{2}(-\boldsymbol{x}_a + \boldsymbol{x}_b - \boldsymbol{x}_c + \boldsymbol{x}_d)$$

where the subscript denotes the numbers of the vertices of the tetrahedron. Again the map is affine. Thus, by solving for (ξ, η, ζ) we may immediately determine the basis functions in physical coordinates, associated with the point values of a scalar function at the center of the edges on the tetrahedron.

To define the new finite element, let $\mathcal{T}_h$ be a conforming, shape regular tetrahedrization of Ω, let $\mathcal{F}_h$ denote the set of all element faces, $\mathcal{F}_h^{\text{int}}$ the faces not on the boundary, and $\mathcal{E}_h$ the set of all element edges in the mesh. We introduce the non-conforming finite element space constructed from the basis previously discussed by defining

$$V_h := \{v : v|_K \in [Q_1^{\text{R}}(\hat{K})] : v \text{ is continuous at the midpoint of } E,\ \forall E \in \mathcal{E}_h\}, \tag{1}$$

For this approximation we have the following property.

Proposition 1 *Denoting by* $[v]$ *the jump across internal faces* $F \in \mathcal{F}_h^{\text{int}}$ *of* $v \in V^h$*, we have*

$$\int_F [v]\, dA = 0. \tag{2}$$

PROOF. Due to the affinity of the map from the reference configuration, the approximation is at most a second degree polynomial at F. A second degree polynomial is exactly integrated by quadrature points in the midpoint of the edges, precisely the points where v has zero jump. Thus the jump integrates to zero over F.

We next introduce the edge based interpolation operator $\pi_h u$ constructed by taking the discrete function that matches the function $u \in H^2(\Omega)$ at the midpoints $\boldsymbol{x}_m$ of the edges. Since the basis includes polynomials complete to first degree and by the existence of a reference element from which we can scale, we have, by the Bramble–Hilbert Lemma (cf. [1]), the following basic estimates:

$$\|u - \pi_h u\|_{L_2(\Omega)} \leq Ch^2 \|u\|_{H^2(\Omega)}, \tag{3}$$

and

$$\|u - \pi_h u\|_{1,h} \leq Ch \|u\|_{H^2(\Omega)}, \tag{4}$$

where

$$\|u\|_{1,h} = \left(\sum_{K \in \mathcal{T}_h} \|u\|^2_{H^1(K)} \right)^{1/2}$$

and h denotes the meshsize. This element thus has the properties necessary to prove optimal *a priori* convergence estimates for standard elliptic problems. We shall next give the details for a particular example, the elasticity problem, which is the main application for this element.

3 Application to the elasticity problem

3.1 Problem formulation and finite element approximation

We consider the equations of linear elasticity describing the deplacement of an elastic body occupying a domain Ω in $\mathbb{R}^3$: find the displacement $\boldsymbol{u} = [u_i]_{i=1}^3$ and the symmetric stress tensor $\boldsymbol{\sigma} = [\sigma_{ij}]_{i,j=1}^3$ such that

$$\begin{cases} \boldsymbol{\sigma} = \lambda \, \nabla \cdot \boldsymbol{u} \boldsymbol{I} + 2\mu \boldsymbol{\varepsilon}(\boldsymbol{u}) & \text{in } \Omega, \\ -\nabla \cdot \boldsymbol{\sigma} = \boldsymbol{f} & \text{in } \Omega, \\ \boldsymbol{u} = \boldsymbol{0} & \text{on } \partial\Omega_{\mathrm{D}}, \\ \boldsymbol{n} \cdot \boldsymbol{\sigma} = \boldsymbol{h} & \text{on } \partial\Omega_{\mathrm{N}}. \end{cases} \tag{5}$$

Here $\boldsymbol{\varepsilon}(\boldsymbol{u}) = [\varepsilon_{ij}(\boldsymbol{u})]_{i,j=1}^3$ is the strain tensor with components

$$\varepsilon_{ij}(\boldsymbol{u}) = \frac{1}{2}\left(\frac{\partial u_i}{\partial x_j} + \frac{\partial u_j}{\partial x_i}\right),$$

$\nabla \cdot \boldsymbol{\sigma} = \left[\sum_{j=1}^3 \partial \sigma_{ij}/\partial x_j\right]_{i=1}^3$, $\boldsymbol{I} = [\delta_{ij}]_{i,j=1}^3$ with $\delta_{ij} = 1$ if $i = j$ and $\delta_{ij} = 0$ if $i \neq j$, $\boldsymbol{f}$ and $\boldsymbol{h}$ are given loads, and $\boldsymbol{n}$ is the outward unit normal to $\partial\Omega$. Furthermore, λ and μ are the Lamé constants, satisfying $0 < \mu_1 < \mu < \mu_2$ and $0 < \lambda < \infty$. In terms of the modulus of elasticity, E, and Poisson's ratio, ν, we have that $\lambda = E\nu/((1+\nu)(1-2\nu))$ and $\mu = E/(2(1+\nu))$. Introducing the space

$$W := \{\boldsymbol{v} : \boldsymbol{v} \in [H^1(\Omega)]^3 : \boldsymbol{v} \text{ is zero on } \partial\Omega_{\mathrm{D}}\},$$

the weak form of (5) can be written: find $\boldsymbol{u} \in W$ such that

$$a(\boldsymbol{u}, \boldsymbol{v}) = (\boldsymbol{f}, \boldsymbol{v})_\Omega + (\boldsymbol{h}, \boldsymbol{v})_{\partial\Omega_{\mathrm{N}}} \quad \forall \boldsymbol{v} \in W, \tag{6}$$

where

$$a(\boldsymbol{u}, \boldsymbol{v}) := \int_\Omega \boldsymbol{\sigma}(\boldsymbol{u}) : \boldsymbol{\varepsilon}(\boldsymbol{v}) \, dV, \tag{7}$$

where $\boldsymbol{\sigma} : \boldsymbol{\tau} = \sum_{ij} \sigma_{ij}\tau_{ij}$ denotes tensorial contraction, and $(\cdot, \cdot)_S$ denotes the L_2 scalar product over S.

To define the finite element method, we introduce the non-conforming finite element space constructed from the space V_h in (1) by defining

$$W_h := \{\boldsymbol{v} : \boldsymbol{v}|_K \in [V_h]^3 : \boldsymbol{v} \text{ is zero at the midpoint of edges on } \partial\Omega_{\mathrm{D}}\}.$$

The finite element method is to find $\boldsymbol{u}_h \in W_h$ such that

$$a_h(\boldsymbol{u}_h, \boldsymbol{v}) = (\boldsymbol{f}, \boldsymbol{v})_\Omega + (\boldsymbol{h}, \boldsymbol{v})_{\partial\Omega_{\mathrm{N}}} \quad \forall \boldsymbol{v} \in W_h. \tag{8}$$

Here

$$a_h(\boldsymbol{u}, \boldsymbol{v}) := \sum_{K \in \mathcal{T}_h} \int_T \boldsymbol{\sigma}(\boldsymbol{u}) : \boldsymbol{\varepsilon}(\boldsymbol{v})\, dV \tag{9}$$

has to be written as a sum over the elements due to the nonconformity of the approximation.

3.2 A priori *error estimates*

We first remark that there is no problem with coercivity with this element as long as at least one face is situated on $\partial\Omega_{\mathrm{D}}$ since we can then stop rigid body rotations by having the displacement prescribed in three (non-colinear) nodes. The element thus fulfills a discrete Korn's inequality, cf. Wang Ming [7]. This not the case, e.g., for the Crouzeix-Raviart [2] and Rannacher–Turek [5] elements (which are typically used for the version of Stokes problem in which the Laplace operator is employed and need stabilization for elasticity, cf. Hansbo and Larson [3]).

Introducing the norm $\|\boldsymbol{u}\|_h := \sqrt{a_h(u,u)}$ we have the following basic estimate.

Proposition 2 *Suppose* $\boldsymbol{u} \in [H^2(\Omega)]^3 \cap W$ *solves (6) and* $\boldsymbol{u}_h \in W_h$ *solves (8). Then*

$$\|\boldsymbol{u} - \boldsymbol{u}_h\|_h \le Ch\|\boldsymbol{u}\|_{H^2(\Omega)}, \tag{10}$$

where the constant C *depends only on the material data.*

PROOF. By Strang's lemma we have that

$$\|\boldsymbol{u} - \boldsymbol{u}_h\|_h \le C\left(\inf_{\boldsymbol{v} \in W_h} \|\boldsymbol{u} - \boldsymbol{v}\|_h + \sup_{\boldsymbol{w} \in W_h} \frac{|a_h(\boldsymbol{u} - \boldsymbol{u}_h, \boldsymbol{w})|}{\|\boldsymbol{w}\|_h}\right)$$

for $\|\boldsymbol{w}\|_h \neq 0$. The first term is of the right order according to (4). The second term can be estimated as follows. We have that

$$\begin{aligned} a_h(\boldsymbol{u}, \boldsymbol{w}) &= \sum_{T \in \mathcal{T}_h} \int_T \boldsymbol{\sigma}(\boldsymbol{u}) : \boldsymbol{\varepsilon}(\boldsymbol{w})\, dV \\ &= \int_\Omega (-\nabla \cdot \boldsymbol{\sigma}(\boldsymbol{u})) \cdot \boldsymbol{w}\, dV + \sum_{F \in \mathcal{F}_h} \int_F (\boldsymbol{\sigma}(\boldsymbol{u}) \cdot \boldsymbol{n}) \cdot [\boldsymbol{w}]\, dA \end{aligned}$$

where $\boldsymbol{n}$ denotes the normal vector taken in the direction of the jump. Here the jump is zero on faces on $\partial\Omega_{\mathrm{N}}$ and equal to $\boldsymbol{w}$ on faces on $\partial\Omega_{\mathrm{D}}$. By (5) and (8) we thus have

$$a_h(\boldsymbol{u} - \boldsymbol{u}_h, \boldsymbol{w}) = \sum_{F \in \mathcal{F}_h} \int_F (\boldsymbol{\sigma}(\boldsymbol{u}) \cdot \boldsymbol{n}) \cdot [\boldsymbol{w}]\, dA.$$

Since the jumps have zero mean, we find, with $\boldsymbol{t} := \boldsymbol{\sigma}(\boldsymbol{u}) \cdot \boldsymbol{n}$, that

$$\begin{aligned} \sum_{F \in \mathcal{F}_h} \int_F \boldsymbol{t} \cdot [\boldsymbol{w}]\, dA &= \sum_{F \in \mathcal{F}_h} \int_F (\boldsymbol{t} - \boldsymbol{c}_1 \boldsymbol{t}) \cdot [\boldsymbol{w} - \boldsymbol{c}_2]\, dA \\ &\leq \sum_{F \in \mathcal{F}_h} \|\boldsymbol{t} - \boldsymbol{c}_1\|_{L_2(F)} \|[\boldsymbol{w} - \boldsymbol{c}_2]\|_{L_2(F)} \end{aligned}$$

where $\boldsymbol{c}_1$ and $\boldsymbol{c}_2$ denotes arbitrary constant vectors on each F. Further, using the trace inequality (proven again by scaling from the reference element, cf. [6])

$$\|v\|^2_{L_2(\partial K)} \leq C\Big(h_K^{-1} \|v\|^2_{L_2(K)} + h_K \|v\|^2_{H^1(K)}\Big), \quad \forall v \in H^1(K), \tag{11}$$

we see that, with $\boldsymbol{c}_1$ chosen as the projection of $\boldsymbol{t}$ onto piecewise constants,

$$\sum_{F \in \mathcal{F}_h} \|\boldsymbol{t} - \boldsymbol{c}_1\|_{L_2(F)} \leq C h^{1/2} \|\boldsymbol{u}\|_{H^2(\Omega)},$$

and by the inverse inequality

$$\|\boldsymbol{v}\|^2_{L_2(\partial T)} \leq C h_T^{-1} \|\boldsymbol{v}\|^2_{L_2(T)}, \quad \forall \boldsymbol{v} \in W_h, \tag{12}$$

we find that, with $\boldsymbol{c}_2$ chosen as the projection of $\boldsymbol{w}$ onto piecewise constants and using Korn's inequality,

$$\sum_{F \in \mathcal{F}_h} \|[\boldsymbol{w} - \boldsymbol{c}_2]\|_{L_2(F)} \leq C h^{1/2} \|\boldsymbol{w}\|_h.$$

Thus,

$$|a_h(\boldsymbol{u}-\boldsymbol{u}_h,\boldsymbol{w})| \le Ch\|\boldsymbol{u}\|_{H^2(\Omega}\|\boldsymbol{w}\|_h$$

and the Proposition follows.

Proposition 3 *Under the assumptions of Proposition 3, assuming $\partial\Omega_D = \emptyset$ and that the domain is smooth enough, we have*

$$\|\boldsymbol{u}-\boldsymbol{u}_h\|_{L_2(\Omega)} \le Ch^2\|\boldsymbol{u}\|_{H^2(\Omega)}, \tag{13}$$

again with C depending on the material data.

PROOF. Consider the auxiliary problem of finding $\boldsymbol{z}$ such that

$$-\nabla\cdot\boldsymbol{\sigma}(\boldsymbol{z}) = \boldsymbol{u}-\boldsymbol{u}_h \quad \text{in } \Omega, \quad \boldsymbol{z}=0 \quad \text{on } \partial\Omega.$$

Assuming $\partial\Omega$ is smooth enough to allow the regularity estimate

$$\|\boldsymbol{z}\|_{H^2(\Omega)} \le C\|\boldsymbol{u}-\boldsymbol{u}_h\|_{L_2(\Omega)}, \tag{14}$$

we have

$$\begin{aligned}\|\boldsymbol{u}-\boldsymbol{u}_h\|^2 &= (\boldsymbol{u}-\boldsymbol{u}_h, -\nabla\cdot\boldsymbol{\sigma}(\boldsymbol{z}))_\Omega \\ &= a_h(\boldsymbol{u}-\boldsymbol{u}_h,\boldsymbol{z}) - \sum_{F\in\mathcal{F}_h}\int_F (\boldsymbol{\sigma}(\boldsymbol{z})\cdot\boldsymbol{n})\cdot[\boldsymbol{u}-\boldsymbol{u}_h]\,dA\end{aligned}$$

Here we can estimate as previosly, using also (14),

$$\begin{aligned}\sum_{F\in\mathcal{F}_h}\int_F (\boldsymbol{\sigma}(\boldsymbol{z})\cdot\boldsymbol{n})\cdot[\boldsymbol{u}-\boldsymbol{u}_h]\,dA &\le Ch\|\boldsymbol{z}\|_{H^2(\Omega}\|\boldsymbol{u}-\boldsymbol{u}_h\|_h \\ &\le Ch^2\|\boldsymbol{u}-\boldsymbol{u}_h\|_{L_2(\Omega)}\|\boldsymbol{u}\|_{H^2(\Omega)},\end{aligned}$$

and we further have

$$\begin{aligned}a_h(\boldsymbol{u}-\boldsymbol{u}_h,\boldsymbol{z}) &= a_h(\boldsymbol{u}-\boldsymbol{u}_h,\boldsymbol{z}-\pi_h\boldsymbol{z}) - \sum_{F\in\mathcal{F}_h}\int_F (\boldsymbol{\sigma}(\boldsymbol{u})\cdot\boldsymbol{n})\cdot[\boldsymbol{z}-\pi_h\boldsymbol{z}]\,dA \\ &\le \|\boldsymbol{z}-\pi_h\boldsymbol{z}\|_h\left(\|\boldsymbol{u}-\boldsymbol{u}_h\|_h + Ch\|\boldsymbol{u}\|_{H^2(\Omega}\right) \\ &\le Ch^2\|\boldsymbol{z}\|_{H^2(\Omega}\|\boldsymbol{u}\|_{H^2(\Omega} \\ &\le Ch^2\|\boldsymbol{u}-\boldsymbol{u}_h\|_{L_2(\Omega)}\|\boldsymbol{u}\|_{H^2(\Omega)}.\end{aligned}$$

The result follows.

4 Numerical examples

To verify the convergence estimate, we first consider the unit cube $[0,1]^3$ with prescribed displacements on all sides and volume load corresponding to the exact solution given by

$$u_x = u_y = u_z = (1-x)x(1-y)y(1-z)z.$$

With $\nu = 0.25$ and $E = 10^3$ we obtain second order convergence in L_2 as shown in Fig. 5.

Our second example concerns material locking and underintegration of the term related to λ as λ becomes large ($\nu \to 0.5$). Though it is likely that this element behaves like a standard Q_1 element with respect to locking (so that it for example cannot safely be used with $P0$ pressures for Stokes), one point integration should alleviate locking in many circumstances. We compare the solution (shown L_2-projected onto the space of linears) for the rotated Q_1 approximation with one point integration in the λ–related term with a linear approximation for the domain with corners in the plane at $(0,0)$, $(4.8,4.4)$, $(4.8,6)$ and $(0,4.4)$. This domain is then extruded in the $z-$direction from $z = 0$ to $z = 0.3$. In Fig. 6 We show the displacements for the linear and rotated Q_1 at $\nu = 0.45$ and in Fig. 7 at $\nu = 0.49$. In these computations, $\boldsymbol{f} = (0,-1,0)$, $E = 10^3$, and the solid was fixed at $x = 0$. The marked locking of the linear element is alleviated with the underintegrated rotated Q_1 element. Finally in Fig. 8 we compare the behavior in locking of the linear, rotated Q_1 and rotated Q_1 with underintegration. Note that only the underintegrated element is locking free, as expected.

Our third example concerns bending. We bend the unit plate of thickness 0.1 by a unit volume load. The material parameters where $\nu = 0.25$ and $E = 10^3$. The plate is fixed at $x = 0$. In Fig 9 we give the linear solution and the Q_1 solution in the same scale. The spurious bending stiffness of the linear element is marked. For comparison, we give the solution using piecewise quadratic polynomials in Fig. 10.

5 Concluding remarks

We have proposed a rotated Q_1 tetrahedral element for elasticity. The element performs better than its linear counterpart in bending and allows for underintegration for avoiding material locking.

References

[1] S.C. Brenner, R.L. Scott, The Mathematical Theory of Finite Element Methods, Springer, New York, 1994.

[2] M. Crouzeix, P.-A. Raviart, Conforming and nonconforming finite element methods for solving the stationary Stokes equations, Rev. Française Automat. Informat. Recherche Opérationnelle Sér. Rouge 7 (1973) 33–75.

[3] P. Hansbo, M.G. Larson, Discontinuous Galerkin and the Crouzeix-Raviart element: Application to elasticity, ESAIM: Math. Model. Numer. Anal. 37 (2003) 63–72.

[4] P.N. Oliver, Pierre Varignon and the parallelogram theorem, Math. Teacher 94 (2001) 316–319.

[5] R. Rannacher, S. Turek, Simple nonconforming quadrilateral Stokes element, Numer. Methods Partial Differential Equations 8 (1992) 97–111.

[6] V. Thomée, Galerkin Finite Element Methods for Parabolic Problems. Springer-Verlag, Berlin, 1997.

[7] Wang Ming, The generalized Korn inequality on nonconforming finite element spaces, Chinese J. Numer. Math. Appl. 16 (1994) 91–96.

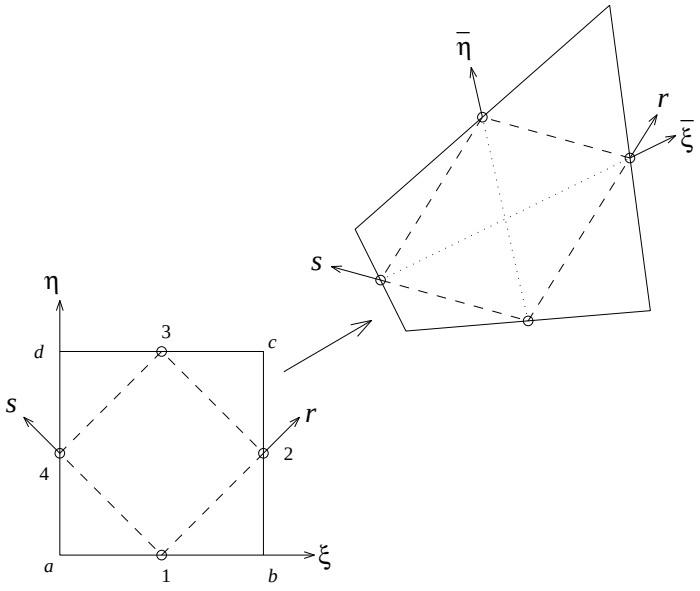

Fig. 1. Reference element $\hat{K}$ and the different coordinate systems used.

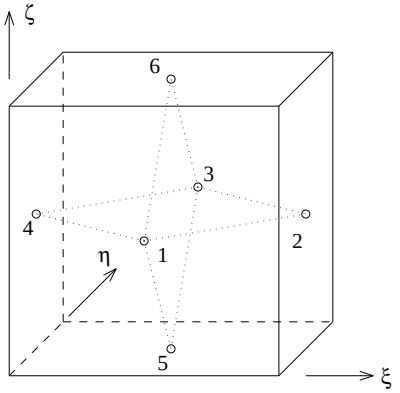

Fig. 2. Reference hexahedron.

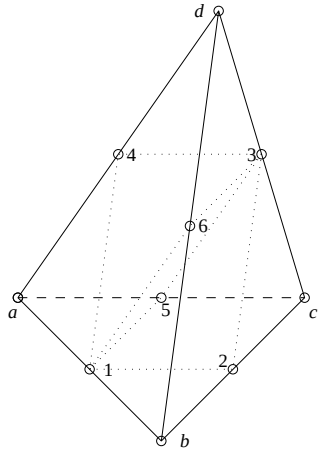

Fig. 3. Physical element K.

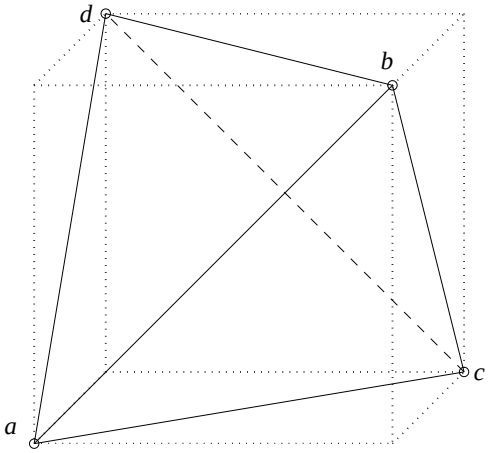

Fig. 4. Reference element $\hat{K}$ inscribed in the hexahedron of Fig. 2.

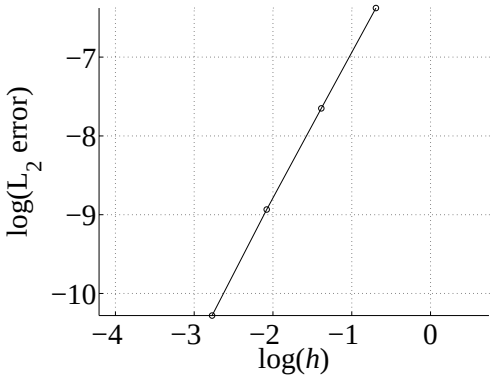

Fig. 5. Convergence in L_2 for a smooth solution.

Fig. 6. Linear solution (left) and rotated Q_1 (right) for $\nu = 0.45$.

Fig. 7. Linear solution (left) and rotated Q_1 (right) for $\nu = 0.49$.

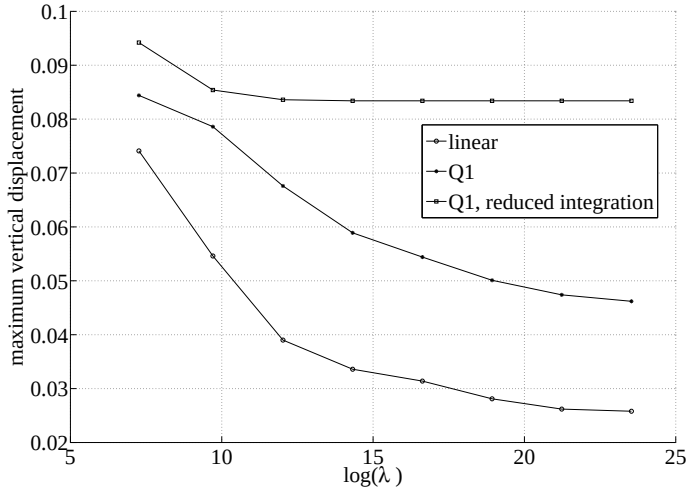

Fig. 8. Locking behaviour for different schemes.

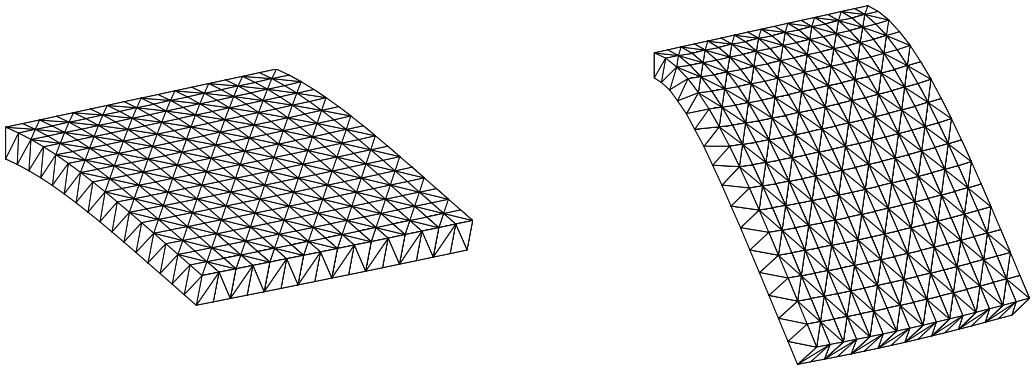

Fig. 9. Bending solution for linears (left) and rotated Q_1 (right).

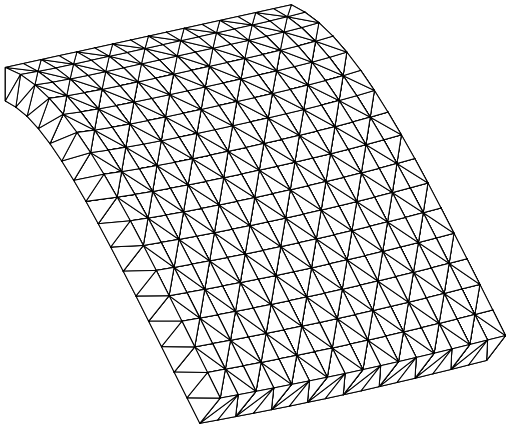

Fig. 10. Bending solution for quadratic polynomials.